Graphite-supported Pt$_n$ Cluster Electrocatalysts: Major Change of Active Sites as a Function of the Applied Potential

Julen Munarriz,[a,b] Zisheng Zhang,[a] Philippe Sautet,[a,c,d,] Anastassia N. Alexandrova [a,c,*]*

[a] Department of Chemistry and Biochemistry, University of California, Los Angeles, 607 Charles E. Young Drive, Los Angeles, CA 90095–1569 (USA).

[b] Departamento de Química Física y Analítica, Universidad de Oviedo, Julián Clavería n° 8, Campus Universitario de El Cristo Oviedo, 33006 (Spain).

[c] California NanoSystem Institute, University of California, Los Angeles, 607 Charles E. Young Drive, Los Angeles, CA 90095–1569 (USA).

[d] Department of Chemical and Biomolecular Engineering, University of California, Los Angeles, 5531 Boelter Hall, Los Angeles, California 90095 (USA).

ABSTRACT. The oxygen reduction reaction (ORR) plays a key role in renewable energy transformation processes. Unfortunately, it is inherently sluggish, which greatly limits its industrial application. Sub-nano cluster-decorated electrode interfaces are promising candidate ORR

electrocatalysts. However, understanding the nature of the active sites on these catalysts in electrocatalytic conditions presents a formidable challenge for both experiment and theory, due to their dynamic fluxional character. Here, we combine global optimization with the electronic Grand Canonical DFT to elucidate the structure and dynamics of sub-nano Pt_n clusters deposited on electrified graphite. We show that under electrochemical conditions, these clusters exist as statistical ensembles of multiple states, whose fluxionality is greatly affected by the applied potential, electrolyte, and adsorbate coverage. The results reveal the presence of potential-dependent active sites, and hence, reaction energetics.

INTRODUCTION

The progressive fossil fuels depletion in conjunction with the need for reducing environmental pollution has motivated an increasing interest in the search for renewable and efficient energy processes.[1] Electrocatalysis plays a crucial role in this field, as it is at the heart of many state-of-the art energy technologies such as fuel cells,[2] hydrogen producing devices,[3] and photovoltaic systems.[4] In this context, (sub-nano) Pt-based clusters are promising catalysts for important electrocatalytic process such as the Oxygen Reduction Reaction (ORR).[5-10] However, they are complex systems, which exhibit many intriguing features that make their study a challenge. Namely, the activity and selectivity of size-selected Pt_n (n = 1–14) clusters deposited on glassy carbon and indium tin oxide depend strongly and non-monotonically on the cluster size.[11-15] Moreover, one key feature of size-selected supported Pt_n clusters is their high fluxional character, which leads to various competing low energy structures. This results in their capability to change shape from thermal fluctuations, and to restructure in response to the number and nature of the

adsorbates. One consequence is that they can circumvent the generally accepted scaling relations of ORR.[16-18]

In electrochemical processes, the catalytic interface can be highly impacted by the applied potential. For example, Reuter and co-workers showed from first principles that the electrode potential causes reconstruction of IrO_2 nanoparticles;[19] and Roldan *et al.* showed a significant restructuring of Cu nanoparticles in CO_2 electro-reduction conditions.[20] Many catalytic intermediates also exhibit potential-dependent coordination modes, such as pyridine on Au(111),[21] oxalate on Ni(111),[22] and activated CO_2 on Cu(211).[23] These observations, in conjunction with the high fluxionality, and structural sensitivity of Pt clusters to the reaction conditions,[24] are suggestive of: *a)* several structures and hence active sites present under given electrochemical conditions, and *b)* a strong dependence of these available active site(s) on the electrochemical conditions on a cluster-decorated interface.

Notice that, at an electrochemical interface, the number of electrons is not fixed, as the electrode acts as a source (cathode) or sink (anode) of electrons. Instead, it is the electrochemical potential that stays constant throughout the chemical reaction. Also, sub-nano clusters are, as other molecular systems, known to adopt different shapes in their different charge state (cationic, neutral, or anionic). Thus, we expect that the explicitly included electrochemical potential should produce significant alterations of the cluster-decorated electrocatalytic interface; as pointed out by us in a recent exploratory work.[25] This way, the central goal of this study is the elucidation of the structural evolution, reagent coverage, and resultant ORR activity of sub-nano Pt clusters deposited on carbon-based electrodes, in the presence of an applied potential and for various adsorbate coverages.

The methodology suitable for this task requires a special note. While previous studies addressed ORR on graphite/graphene supported Pt clusters,[26-30] the global optimization typically required for small clusters has barely been accomplished under electrochemical conditions. At this point, we should comment on the work of Nakajima and co-workers, who have studied graphite-based surfaces decorated with Pt_n clusters by pre-optimizing the clusters in the gas phase and then depositing them in the surface, the potential effect being later included by means of the Computational Hydrogen Electrode (see below). In order to identify the relevant clusters at working conditions, they relied on XAFS spectroscopy, and used it to match the observations with some of the DFT computed structures.[15,31] Even though their approach is, without any doubt, valuable, they had to recur to experimental evidence to identify the global minimum (GM), and did not consider ensemble effects. In this sense, our perspective is different, as it is enforced to extract the chemical information from simulations without requiring external input.

Indeed, accounting for the potential-dependent effects in adsorption and especially fluxionality is not trivial, and cannot be done, for example, within the widely-used Computational Hydrogen Electrode (CHE) model.[32] In this work, we therefore combine global optimization techniques with an explicit grand canonical modelling of the electrochemical potential, which employs the surface charging (SC) technique combined with the linearized Poisson−Boltzmann (PB) implicit solvation model as reported in ref. 21. Adding full explicit solvation and the sufficient statistical mechanical sampling of the solvent and ions to the scheme would be prohibitively expensive.[33] Therefore, we resort to implicit solvation with the PB model of the electrolyte[34] - the approach has demonstrated success for a variety of electrochemical processes.[21,35,36] We note that some authors have reported that linearized Poisson-Boltzmann models cannot provide a fully satisfactory description of electrolyte-electrode interfaces.[37] Nonetheless, our main focus is on the geometry of Pt_n clusters

and its dependence on the applied potential, rather than on the specific electrolyte-electrode interaction, and we expect that the conclusions extracted from this work will hold when applying more elaborate electrochemical models. In this regard, we highlight that modelling the electrochemical reconstruction of interfaces is very challenging, and new theoretical methods continue to be developed.[37-45]

We studied the effect of the applied potential on the ensemble composition of Pt_n (n = 3, 5) size-selected sub-nano clusters deposited over graphite and in the presence of relevant intermediates of ORR (for Pt_5 systems). We selected graphite as a model system for the support, which is generally based on amorphous carbon-based structures, an approach that has been applied by us, as well as other authors (either using graphite or graphene).[15,16,25] Herein, we do not address the effect of the Pt-support interaction in heterogeneous supports due to computational limitations, which has been addressed by other authors;[46-50] nonetheless, we expect our main conclusions to qualitatively hold independently of the support. We note that some recent works have computationally studied the potential dissolution of Pt clusters in acidic environments,[51] as well as sintering effects,[52] and the stability of other electrocatalytic systems under different electrocatalytic conditions.[53] We also highlight that mono-disperse ensembles of Pt clusters adsorbed on a variety of surfaces have been experimentally prepared and are therefore worth exploring to better understand such systems,[5,6,11-15] without prejudice to the analysis of the aforementioned effects, which, although worth-exploring, are out of the scope of this work – in which we aim to analyze cluster fluxionality as a function of the applied potential.

Overall, we believe our approach is innovative and can offer a significant advance in the understanding of dynamic electrochemical catalytic interfaces.

RESULTS AND DISCUSSION

The structures for the global optimizations were generated by our in-house code, PGOPT, with bond length distribution algorithm (BLDA),[54] and optimized with dispersion-corrected DFT in the presence of an electrostatic potential (with respect to the standard hydrogen electrode), U*(SHE)*. We selected an electrolyte concentration of 1 M and analyzed the electrochemical potential in the [0 – 1.2] V range. We start with the potential dependence of bare clusters, the presence of adsorbates being presented later. This is a purely theoretical view, since clusters will be adsorbate covered at many potential values. At negative potentials they are expected to be covered by hydrogen, and hydrogen evolution reaction will take place. Hydrogen coverage is also expected at small positive potentials due to well-known hydrogen under-potential deposition, which is a consequence of a strong interaction between hydrogen and the Pt in the cluster.[55,56] Nonetheless, the analysis in the full (hypothetical) range allows gauging a baseline of the possible extent of cluster fluxionality under the applied potential, and we expect this base-line dynamics to affect the system behavior in the presence of relevant adsorbates. The full description of the computational details is provided in the Supporting Information.

Pt_1 and Pt_2 clusters. Pt_1 and Pt_2 clusters over a graphite surface are considered first. All the initial structures of Pt_1 converged to the same minimum, in which Pt is in the bridging position over a single C–C bond (Figure S1a). This adsorption mode has been reported by other authors.[26,57] For Pt_2 structures, we also found a single predominant coordination mode, in which the Pt atoms lie over two C–C bonds belonging to adjacent hexagonal rings (Figure S1b). The predicted potential dependence of these structures is minimal.

Pt$_3$ clusters. Pt$_3$ clusters have a more diverse conformational distribution: Five different local minima were found within the energy cutoff with respect to the GM of 0.7 eV, when no applied potential is included. The energy cutoff was chosen generously to account for the possible differential (de)stabilization of the isomers when the potential is applied. The various structures are labeled as Pt$_3$-#min, where #min indicates the stability order with respect to the GM when the potential effect is not considered (neutral system), and this nomenclature is kept for the following systems.

All the structures are Pt triangles, whose dimensions and adsorption sites on the support differ slightly (Figure 1a). The four most stable structures are within less than 0.2 eV from the GM. Pt$_3$-V is significantly less stable than the other isomers, and, even when the potential effect is considered, it does not contribute to the overall Boltzmann ensemble at room temperature.

Isomers Pt$_3$-I–Pt$_3$-IV exhibit sensitivity and order switching as a function of the applied potential. Note that, under CHE, the energy difference between the minima would be constant (and equal to that of the neutral system), and their statistical distribution would not change as a function of the potential. This way, the Boltzmann structural ensemble at 300 K would consist of 75% of Pt$_3$-I, 19% of Pt$_3$-II and so on; see P$_{NS}$ entry in Figure 1 – P$_{NS}$ corresponds to the Boltzmann probability when taking the energy results for the neutral systems, which is the basis of the CHE model. In contrast, when we explicitly account for the potential via SC, the picture changes dramatically. For example, the distribution of Pt$_3$-I now varies as a function of the potential, between 15 and 96% at 300 K, which is a typical temperature in electrocatalysis (see Figure 1). We note that the ability to fully rearrange into an equilibrium thermodynamic ensemble in response to the current conditions is assumed in this study. Such an assumption is supported by previous theoretical and experimental findings.[58,59] Namely, some of us proposed on the basis of theoretical

calculations (DFT in conjunction with GO and molecular dynamics simulations) that Pt_7 clusters deposited over Al_2O_3 can very rapidly interconvert.[58] Moreover, interconversion between several isomers of Pt_4 clusters in a graphene-based support has been experimentally detected.[59] Nonetheless, we acknowledge that the generality of this assumption should be investigated in the future, including in the experiment, and that the change in the potential might lead to metastable clusters that are kinetically trapped at some potentials, which could be relevant for the catalysis.

Remarkably, a potential-dependent switch in the GM, between Pt_3-I and Pt_3-II, is observed at -0.6 V. Even though at U(SHE) > -0.6 V the GM remains unchanged (as Pt_3-I), the 300 K populations of various isomers (Pt_3-I to Pt_3-III) change as a function of U(*SHE*) (Figure 1a). In fact, no isomer is fully predominant at any potential, and the ensemble composition can be modified by switching the potential. For example, at 0.3 V the ensemble contains 80% of Pt_3-I, 15% of Pt_3-II and 5% of Pt_3-III. While in this case the structures are relatively similar, these results are relevant, as they show the important effect of the applied potential in governing the cluster probability distribution.

This GM switch is, in broad strokes, a consequence of the potential of zero charge (PZC) difference between the various isomers (i.e. 0.09 V for Pt_3-I and 0.20 V or Pt_3-II), which determines the center of the parabolic dependence of the cluster Gibbs energy *w.r.t.* the potential, as the parabola's curvature (related to the system polarizability, Figure S3) are qualitatively similar. Note that the PZC corresponds to the potential at which the free energy-potential parabola has zero first order derivative with respect to the potential, that is, the location of the maximum. The PZC changes even further for larger and more geometrically diverse clusters (*vide infra*). This difference in the cluster behavior as a function of the potential has been attributed to the differences in the surface dipole moments, which naturally change when the cluster shape changes.[21]

Pt$_5$ clusters. The Pt$_4$/graphite system was addressed in a recent separate study.[25] Pt$_5$ clusters show a growing geometric diversity (Figure 1b and Figure S4). Pt$_5$-I (and also Pt$_5$-III) exhibits a distorted pentagonal geometry, which has previously been attributed to a second order Jahn-Teller effect,[60] hinting at the sensitivity of its stability to the electron count. Indeed, the populations for Pt$_5$-I and Pt$_5$-II range between 53-100% and 0.1-44%, respectively, at 300 K (Figure 1b), following the large variations in the energy gap between these structures with the change of the potential. For instance, at 0.0 V, when Pt$_5$-II is stabilized the most, it is less than 0.01 eV above Pt$_5$-I, which corresponds to 44% of Pt$_5$-II and 53% of Pt$_5$-I at 300 K. Note that there is a region of the potential of a significant co-existence of Pt$_5$-I, Pt$_5$-II and Pt$_5$-III (at 300 K) at about 0.7 V. It might seem surprising that Pt$_5$-I is stabilized at both more positive and more negative potentials. As shown in Figure S5, it is a consequence of the very different curvature of the Gibbs energy *vs* potential parabolic fitting, which is much higher for Pt$_5$-I. If considering the energy data for the neutral systems (CHE model), the populations would stay constant, at 71% of Pt$_5$-I and 23% of Pt$_5$-II.
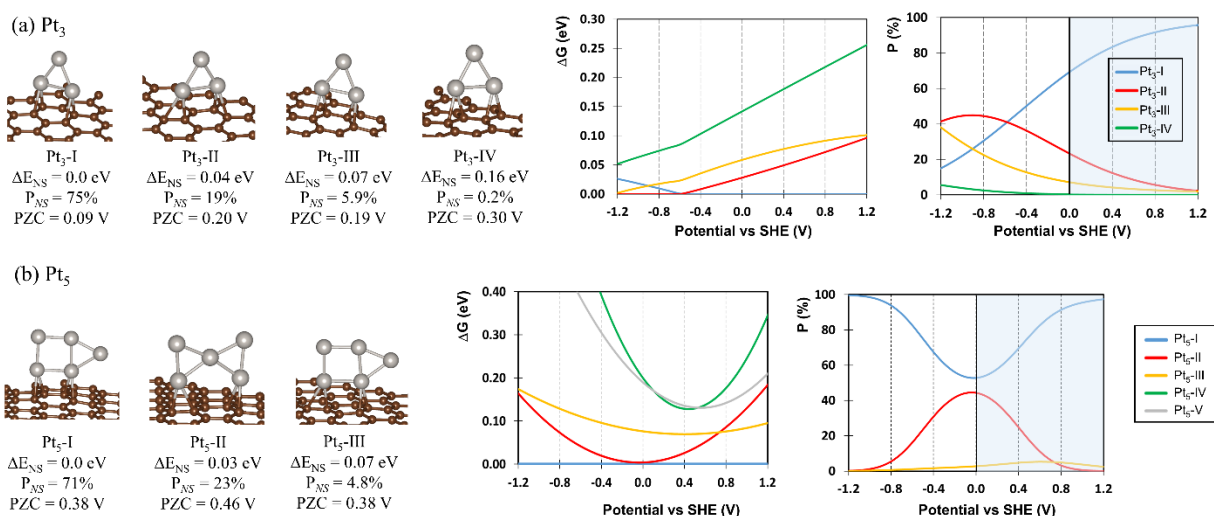
Figure 1. Left: Selected local minima, relative energy with respect to the GM for the neutral systems (ΔE_{NS}), PZC, and Boltzmann cluster populations at 300 K considering the neutral systems

(P_{NS}). Right: ΔG (with respect to the GM at each potential) as a function of the potential (*w.r.t.* SHE), and Boltzmann cluster distribution as a function of the potential at 300 K in the SC framework for: (a) Pt$_3$, (b) Pt$_5$ systems. The more realistic potential range [0.0 – 1.2] V is highlighted in light blue.

Potential- and coverage-dependent ORR energetics on Pt$_5$/graphite. We now focus on the largest cluster considered in this study, Pt$_5$/graphite, and report on the impact of the potential and adsorbate coverage effects on the ORR activity. First, we study the adsorption of the reaction intermediates for the 4-electron ORR mechanism (Scheme 1), *O, *OH, and *OOH.[61] Note that adsorption can be coupled to geometric rearrangements of the cluster, beyond simple relaxation, leading to the reagent itself preparing the real active site possibly absent on the bare catalyst.[16,62-64] Hence, we aim to interrogate how the nature of the active sites changes as a function of the nature and coverage of the bound intermediates, as well as the applied potential, simultaneously.
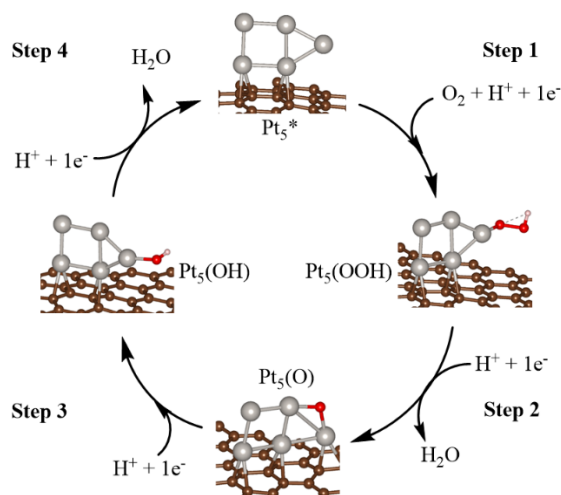

Scheme 1. Schematic representation of the four-electron mechanism of ORR. A model Pt$_5$ cluster with a single adsorbate has been taken as reference for visual purposes.

Pt$_5$ clusters with one adsorbate. Adding one adsorbate dramatically affects the structural morphology of Pt$_5$/graphite. Importantly, the cluster geometry is also potential-dependent (Figure 2a-c). For all three considered adsorbates, *OH, *O and *OOH, the ensemble at 300 K is composed mainly of two different cluster isomers, with potential-dependent proportions.

For Pt$_5$(OH) clusters, we found a potential-dependent GM: Pt$_5$(OH)-I or Pt$_5$(OH)-IV. Although the neutral Pt$_5$(OH)-IV is 0.28 eV above the GM (being the fourth most stable geometry), PZCs for Pt$_5$(OH)-I and Pt$_5$(OH)-IV are significantly different (0.31 and 0.11 V, respectively), and the curvatures in the parabola are also different (Figure S7). As a result, Pt$_5$(OH)-IV becomes dominant at 1.1 V. On the contrary, neutral system results (CHE model) would lead to 99% of Pt$_5$(OH)-I, 1% of Pt5(OH)-II, and no relevant proportions of Pt$_5$(OH)-IV (at 300 K).

For Pt$_5$O clusters, two structures (Pt$_5$O-I and Pt$_5$O-II, Figure 2) are very close in energy, with an energy difference of 0.04 eV for the neutral systems, corresponding to 85% of Pt$_5$O-I and 15% of Pt$_5$O-II at 300 K. Importantly, the SC modelling of the potential induces two switches in the GM, alternating between these two structures (see Figure 2b). The double switch is a consequence of the parabolic shape of the Gibbs energy with the potential, which in this case translates into Pt$_5$O-I being predominant in the [0.1 - 0.8] V range, and Pt$_5$O-II outside of this range. This behavior is attributed to the significantly different values of PZC, but especially to the very different parabola curvature (*i.e.* in the capacitance variation of these clusters), which is much more pronounced for Pt$_5$O-I (see Figure S9).
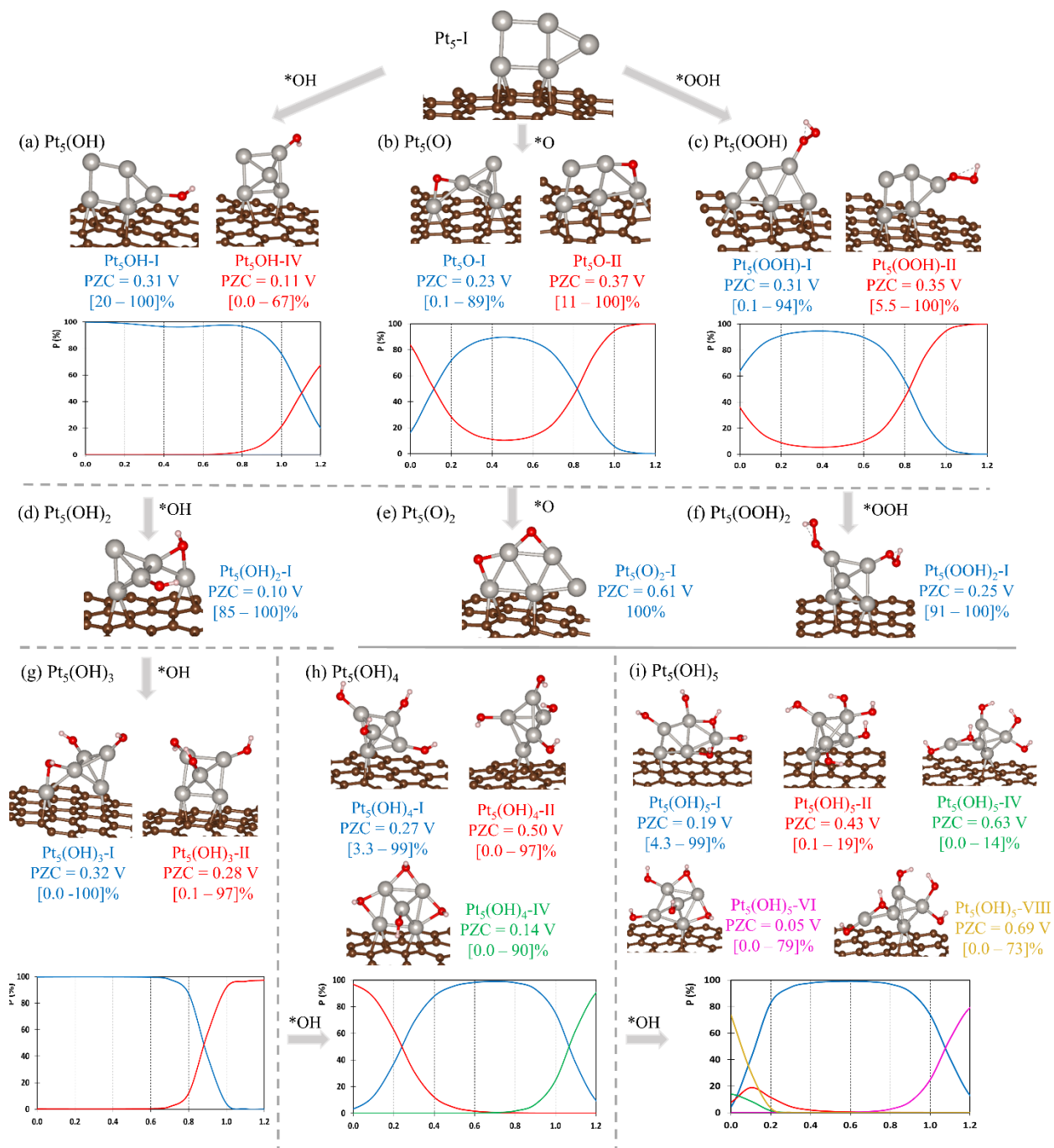
Figure 2. Selected local minima for Pt$_5$-adsorbate systems, PZC and Boltzmann cluster distribution as a function of the potential in the SC framework at 300 K. The *x* axis corresponds to the potentials (vs *SHE*) in unit of V.

The same behavior of alternation between two structures is obtained for $Pt_5(OOH)$ clusters, with two minima, $Pt_5(OOH)$-I and $Pt_5(OOH)$-II (Figure 2c) that are only 0.07 eV apart when the potential effect is not taken into account. This energy difference would correspond to 94% of $Pt_5(OOH)$-I and 6% of $Pt_5(OOH)$-II at 300K. Inclusion of the potential via SC changes the picture: in the [0.0–1.2] V range, the $Pt_5(OOH)$-I population varies from 0.1% to 94% (reaching the maximum at ca 0.4 V), and that of $Pt_5(OOH)$-II ranges between 6 and 100% (reached at *ca.* 1.1 V, see Figure 2). There is a GM switch from $Pt_5(OOH)$ I to $Pt_5(OOH)$-II at *ca.* 0.8 V – again a consequence of the very different parabola curvatures (see Figure S11).

Pt_5 clusters with two adsorbates. Interestingly, additional adsorbates change the GM, and that is especially significant for $Pt_5(OH)_2$ and $Pt_5(OOH)_2$ (Figure 2d and 2f), whose geometrical structures are completely different from those of $Pt_5(OOH)$ and $Pt_5(OH)$. For OH, the preferred binding mode changes from atop to bridge. Contrarily to the previous case, the GM is constant in the entire potential range: 100% of $Pt_5(O)_2$ is in $Pt_5(O)_2$-I (Figure 2e), and 96-100% of $Pt_5(OOH)_2$ is in $Pt_5(OOH)_2$-I (Figure 2f). The collapse of the ensemble to a single structure is a signature of particular stability, reached through adsorbate induced geometric change, and making the adsorption stronger.[65] The potential-dependent geometric variation is somewhat more pronounced for $Pt_5(OH)_2$, where the population of GM, $Pt_5(OH)_2$-I, oscillates between 85 and 100% (Figure 2d). Due to lower structural variation with the potential, the results in this case would be closer to those of the CHE model, which predicts populations of $Pt_5(OOH)_2$-I, $Pt_5(O)_2$-I and $Pt_5(OH)_2$-I of 92%, 100% and 96% at 300 K. Notice also that modeling these catalysts under insufficient coverage apparently can lead to a misrepresentation of the active site.

Pt_5 clusters with three, four and five OH adsorbates. As will be shown below, the analysis of the ORR energetics reveals the fourth step (protonation of *OH to yield water) being

thermodynamically limiting. This is because the *OH binding is the most exothermic for one and two adsorbates (Figure 3), which would lead to the clusters at the catalytic interface being covered by the *OH adsorbates.[61] Hence, we focus on *OH and increase the adsorbate coverage. The third *OH adsorbate reinvigorates the potential-dependence of the GM (Figure 2g). For the neutral systems, $Pt_5(OH)_3$-I is 0.20 eV more stable than $Pt_5(OH)_3$-II, which corresponds to relative proportions of 99.9 and 0.05%, respectively, at 300 K. However, in the more elaborate SC framework, GM switches at 0.9 V from $Pt_5(OH)_3$-I (structurally related to $Pt_5(OH)_2$-I) to $Pt_5(OH)_3$-II. Contrarily to other cases, in which GM switches were associated to significantly different PZCs, in this case the two structures have very similar values of PZC: of 0.32 and 0.28 V, respectively. Nonetheless, the capacitances are very different, as revealed by a significantly higher curvature in the parabola for $Pt_5(OH)_3$-II (see Figure S16), which is responsible of it being more stable from 0.9 V on.

The addition of a fourth *OH adsorbate also brings important consequences for the ensemble composition. GM changes three times as a function of the potential in the studied widow (Figure 2h). The GM for the neutral systems, $Pt_5(OH)_4$-I, is predominant in the [0.25 – 1.1] V range, $Pt_5(OH)_4$-II is GM up to 0.25 V, and $Pt_5(OH)_4$-IV is GM at potential above 1.1 V. Notice that the structural diversity of clusters geometry is reflected in the electrochemical behavior; namely, PZC varies in a wide range: 0.27 V for $Pt_5(OH)_4$-I, 0.50 V for $Pt_5(OH)_4$-II, 0.34 V for $Pt_5(OH)_4$-III, and 0.14 V for $Pt_5(OH)_4$-IV. This, in conjunction with different parabola curvatures (Figure S18), results in the aforementioned stability alteration. The ensemble composition in the CHE picture would be 86% of $Pt_5(OH)_4$-I and 13% of $Pt_5(OH)_4$-II at all potentials at 300 K.

Finally, $Pt_5(OH)_5$ clusters also exhibit a strong geometric dependence on the applied potential (Figure 2i). Namely, in the [0.0 – 1.2] V range, there are three main predominance regions: [0.0 –

0.1], [0.1 – 1.0] and [1.0 – 1.2] V. Between 0 and 0.1 V, $Pt_5(OH)_5$-VIII is the majority, with 73% population at 0 V. Other significant structures in this range are the GM for the neutral systems ($Pt_5(OH)_5$-I), as well as $Pt_5(OH)_5$-II and $Pt_5(OH)_5$-VI. Note that, while $Pt_5(OH)_5$-VIII is 0.23 eV higher in energy than the GM, their PZC values are very different (0.19 V for $Pt_5(OH)_5$-I and 0.69 V for $Pt_5(OH)_5$-VIII, Figure 2i), which, in conjunction with a different curvature in the parabola is responsible for the switch in the potential-dependent GM (Figure S20). In addition, when inspecting Figure 2i, it is clear that $Pt_5(OH)_5$-VI and $Pt_5(OH)_5$-VIII show very similar geometries, only exhibiting subtle differences in interatomic distances. Namely, when considering the neutral systems, $Pt_5(OH)_5$-VI is only 0.02 eV more stable than $Pt_5(OH)_5$-VIII. This way, when including the potential effect via SC, the combination of PZC and parabola's curvature translates into $Pt_5(OH)_5$-VIII being more stable in the considered potential range. Between 0.1 and 1.0 V, $Pt_5(OH)_5$-I, constitutes the majority; while at potentials above 1.0 V, $Pt_5(OH)_5$-VI does. This is mainly attributed to a sharper parabola curvature for $Pt_5(OH)_5$-VI (Figure S20).

The populations at 300 K derived from the CHE approach are: 94% of $Pt_5(OH)_5$-I, 5% of $Pt_5(OH)_5$-II, 0.3% of $Pt_5(OH)_5$-III, and only 0.1% of other clusters; which reveals the large sensitivity of the ensemble composition of the adsorbate decorated electrocatalysts to the applied potential. One complication here is that with 5 adsorbates, we start finding cluster geometries which are less bonded to the support. This might indicate the high propensity for sintering, affecting the practicability of ORR catalysis on Pt_n/graphite.

ORR electrocatalysis on Pt_5/graphite. We now explicitly address the energetics of the ORR steps, with the special focus on the potential-limiting reaction step (step 4 in Scheme 1). The following discussion is based on the system ensemble-averaged adsorption energies (Figure 3), but qualitatively similar conclusions can be drawn when the energies are computed with respect

to the GM at each potential (see Figure S22). We first consider one adsorbate, ensemble binding energies of *O, *OH, and *OOH (ΔG_O, ΔG_{OH}, and ΔG_{OOH}) to Pt$_5$ being shown in the Supporting Information (Figure S21). *OOH shows the least favorable binding, between 2.63 and 3.18 eV (versus 3.14 eV in the CHE framework). Notice that ΔE_{OOH} exhibits a *"shoulder"* at about [0.8 – 1.2] V, due to the GM switching from Pt$_5$(OOH)-I to Pt$_5$(OOH)-II in this region, which affects the relative cluster proportions, and thus the total ensemble energy of the system. ΔG_O are in the range between 0.71 and 0.78 eV (versus 0.72 eV in the CHE framework). Remarkably, ΔG_{OH} is negative, -0.18 eV in CHE, and between -0.13 and -0.21 eV in SC, revealing that Pt$_5$/graphite suffers from over-binding, which is expected to limit the ORR activity and will lead to the catalytic interface being covered with *OH adsorbates.[25]

Based on adsorption energies, we computed ΔG for the four steps of ORR (Scheme 1, ΔG_1 – ΔG_4) as a function of the potential for the system covered by one and two adsorbates (Figure 3a and 3b), and ΔG for the fourth step (ΔG_4) for 1 – 5 *OH adsorbates (Figure 3c). As shown in Figure 3a for the case in which only one adsorbate is considered, due to *OH over-binding, ΔG_4 (protonation of *OH to produce water) is the thermodynamically limiting step of ORR, being positive in the entire potential range, [0 – 1.2] V.[15,25,66] This would suggest that Pt$_5$/graphite is inactive towards ORR catalysis in the considered coverage conditions; as ΔG_4 becomes negative at about -0.1 V, which would correspond to an ORR overpotential higher than 1.23 V. This result resonates with previous calculations on Pt$_5$, which, under an already explained different approach predicted an overpotential of 1.04 V.[15]

(a) One adsorbate

(b) Two adsorbates
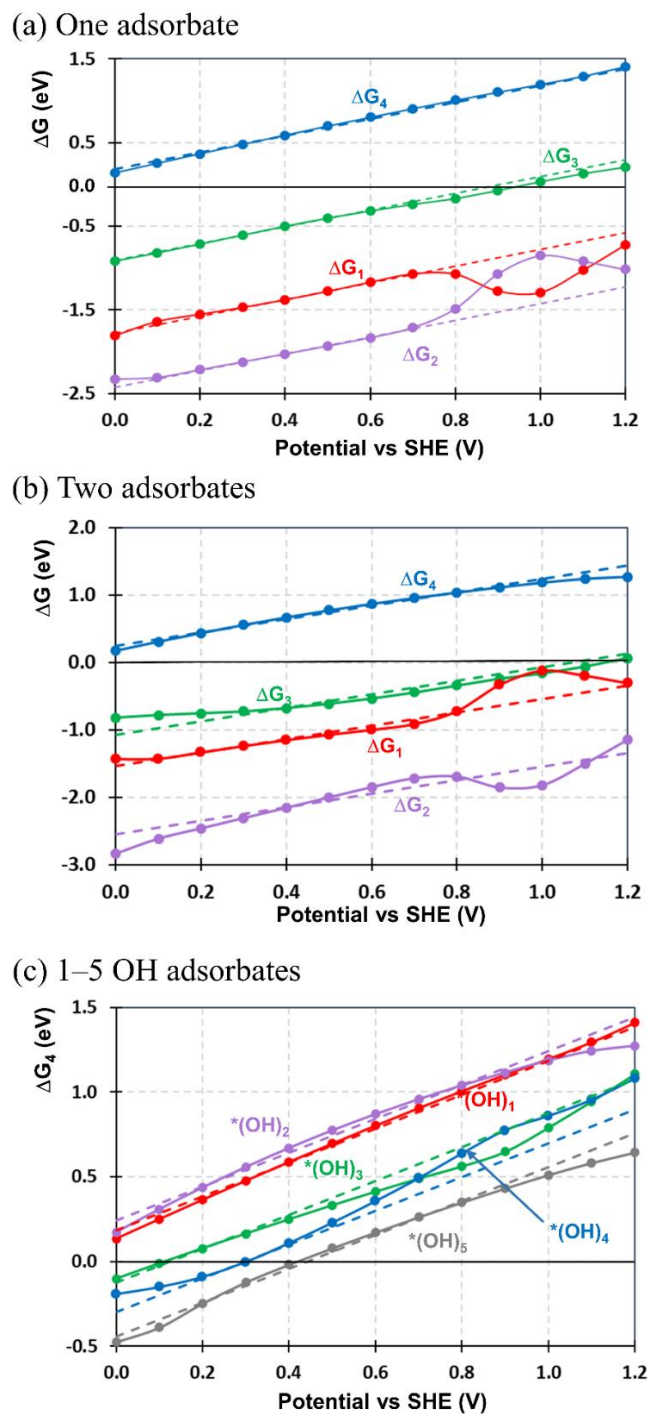
(c) 1–5 OH adsorbates

Figure 3. ΔG for the four steps of the 4-e$^-$ mechanism of ORR of (a) Pt$_5$/graphite with one adsorbate and, (b) two adsorbates. (c) ΔG_4 (ΔG for the fourth step of the 4-e$^-$ mechanism of ORR) of Pt$_5$/graphite with 1 – 5 *OH adsorbates. SC results are shown in solid lines and CHE ones in dotted lines.

When comparing SC and CHE approaches, significant differences between them are found. While they are almost indistinguishable in the low potential range, the GM switching in $Pt_5(OOH)$ translates into important oscillations in ΔG_1 and ΔG_2, even leading to them crossing at 1.0 V. We note that relevant differences between the two approaches had also been proposed by some of us;[61] and other authors have also reported that explicit inclusion of the electrochemical potential in the calculation leads to potential-dependent differences in surface termination and reaction mechanisms.[67-69]

Next, we study how coverage affects the energetics of the reaction steps. We added an extra *O, *OH and *OOH adsorbate to the previous structures; *i.e.* *OH to $Pt_5(OH)$, *OOH to $Pt_5(OOH)$ and *O to $Pt_5(O)$, and computed the binding energies (*w.r.t.* the previous coverage) and the derived ΔG values for the four steps of ORR. We found that the absolute values of the binding energies are relatively similar to those computed for a single adsorbate (see Figure S21a and b). Unfortunately, the binding energy of *OH is roughly the same (even about 0.05 eV more negative at low potentials) as for $Pt_5(OH)$, indicating that this coverage increase does not mitigate the over-binding, and ORR would not take place in the potential range between 0 and 1.23 V (as ΔG_4 is positive, unfavorable in the whole range). Moreover, the negative adsorption energy for *OH, would strengthen the possibility of the real catalytic interface being covered of *OH adsorbates.

Hence, as *OH adsorption is by far more favorable than *O and *OOH, and the ORR thermodynamic-limiting reaction step is #4 – *OH protonation to yield water, we only consider further addition of *OH to the cluster catalyst ensemble (Figure 3c). The third *OH leads to a change in both the binding sites and the cluster shape, which is typical of sub-nano cluster catalysis.[65] This has relevant implications for the energetics of the activity-limiting ORR step.

Specifically, ΔG_{OH} is now positive (about 0.2-0.4 eV increase compared to two adsorbates), indicative of partial mitigation of over-binding. This leads to ΔG_4 (intimately related to $-\Delta G_{OH}$, see Computational Details in the Supporting Information) being negative (favorable) at potentials lower than 0.1 V, which corresponds to an ORR overpotential of 1.12 V, in both CHE and SC approaches. Interestingly, the CHE and SC binding energies (and thus ΔG_4 values) are relatively similar at low potentials (between 0 and 0.3 V, and that is why they lead to similar overpotentials), but differ significantly at potentials higher than 0.3 V. This is a consequence of cluster fluxionality and the parabolic dependence of the system's Gibbs energy on the potential.

ORR energetics are even more favorable upon adsorption of the fourth *OH, which leads to an additional change in the cluster morphology. ΔG_{OH} increases at low potentials, while it is less unfavorable than that derived from three adsorbates at [0.7 − 1.2] V. Notice that ΔG_{OH} in the SC framework deviates significantly from that derived from CHE (see Figure 3c). The increase in ΔG_{OH} at low potentials leads to further decrease in the ORR overpotential. Namely, the ORR onset potential – the potential at which all reaction steps became thermodynamically favorable – would be 0.30 V, corresponding to an overpotential of 0.93 V.

This favorable tendency holds for the fifth adsorbate, which further destabilizes *OH adsorption by about 0.1–0.4 eV (depending on the potential, Figure 3c). The destabilization benefits the fourth ORR step, which now becomes exothermic at 0.4 V, that is, the system would have an ORR overpotential of 0.81 V.

Thus, we can see that increasing cluster coverage reduced ORR overpotential, and, although it keeps being higher than that of Pt(111) (about 0.4 V),[32,70,71] it is indicative of the activity increase. In addition, it should be highlighted that, even though the overpotential of these clusters is higher

than that of Pt(111), the Pt loading in clusters systems is much lower, and the relative surface area and site–specificity to interact with O_2 molecules is higher, which can overcome the overpotential increase in practical applications.[15,72] Note that adsorption energies of *OH point towards the adsorption of the first two adsorbates being thermodynamically favorable, thus revealing that the real catalytic interface will be covered by *OH. In order to assess the potential competition between cluster hydroxylation and ORR, in Figure 4 we compare their relative energetics for U(*SHE*) of 0.4 and 0.8 V. The results show that cluster hydroxylation (*i.e.* steps 1 to 3 of ORR) is the preferred pathway, thus indicating that high cluster coverage is expected for these systems. The extent to which this coverage takes place would also depend on the experimental conditions such as electrolyte concentration (we are not explicitly considering the pH effect in this contribution) and temperature, and is expected to hinder the system performance. Nevertheless, our results reveal how increasing coverage, coupled to cluster restructuring and surface charging, affects the catalytic activity, and how all these effects need to be taken into account to find the actual active site.[73]
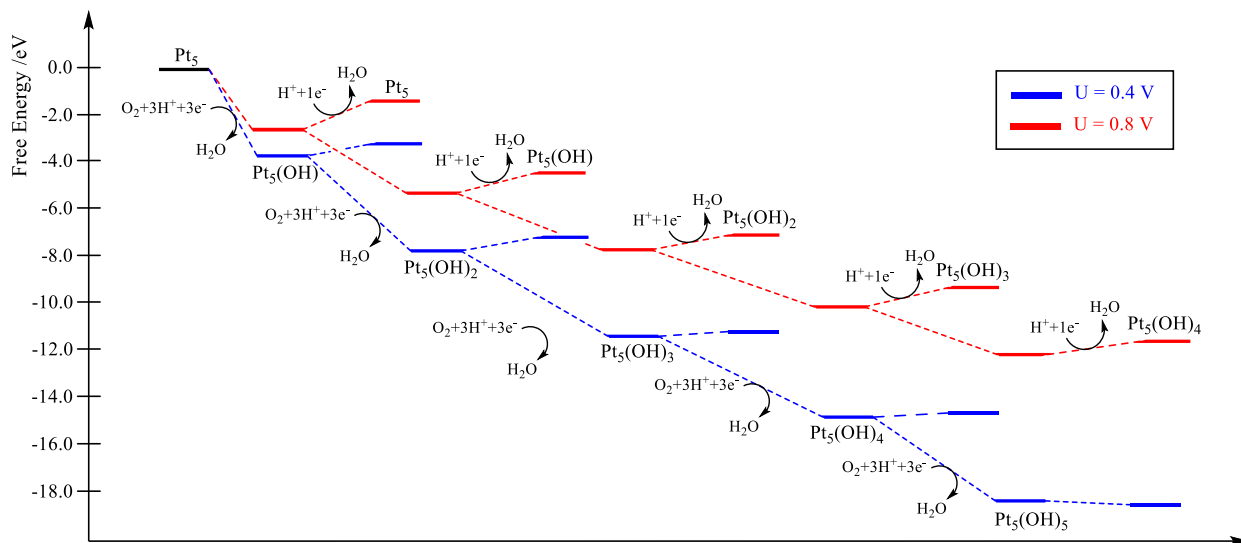
Figure 4. Free energy diagram for ORR and hydroxylation process of Pt_5/graphite at potentials of 0.4 and 0.8 V (*w.r.t* SHE). Steps 1 – 3 of ORR are represented together as $Pt_5(OH)_n + O_2 + 3H^+ + 3e^- \rightarrow Pt_5(OH)_{n+1} + H_2O$.

CONCLUSIONS

This study reveals that an accurate description of cluster-decorated electrochemical interfaces requires for the explicit consideration of the electrochemical potential and the restructuring of the interface at this potential, and in the presence of the adsorbates at relevant coverages. Because of the highly fluxional character of supported sub-nano clusters, they are able to change shapes as a function of the applied potential, so that the dominant species in the cluster population can also be highly potential-dependent. We expect the behavior to be non-monotonic with the Pt cluster size, as Pt_3 and Pt_5 behave differently, and the same happens with different adsorbates coverages for Pt_5 size: some systems show a more pronounced structural sensitivity to the potential. Moreover, the example of Pt_5 with adsorbates highlights the dramatic geometrical change that takes place when adsorbates bind to the clusters in their potential-dependent binding modes. Considering more relevant higher coverages is also evidently crucial for predicting the ORR activity, whereas at lower coverages, the *OH adsorption is too strong and incompatible with the ORR activity. These results have important implications for cluster electrocatalysis, as they highlight the crucial effect of the applied potential on the ensemble composition, thus providing a step toward in the accurate modelling of fluxional electrochemical interfaces, and in the understanding of novel catalysts with switchable properties a function of the potential.

As a final comment, we should note that parameters in the model can affect the absolute values of binding energies and overpotentials. However, the results highlight important phenomena that

must hold true regardless of the model, such as potential-dependent cluster fluxionality and interface restructuring, and, consequently, potential-dependent binding energies and ORR steps energetics (and thus overpotentials).

AUTHOR INFORMATION

Corresponding Authors

Anastassia N. Alexandrova − Department of Chemistry and Biochemistry, University of California, Los Angeles, Los Angeles, California 90095, United States; California Nano Systems Institute, Los Angeles, California 90095-1569, United States; orcid.org/0000-0002-3003-1911; Email: ana@chem.ucla.edu

Philippe Sautet − Department of Chemical and Bio-molecular Engineering, University of California, Los Ange-les, Los Angeles, California 90095, United States; Department of Chemistry and Biochemistry, University of California, Los Angeles, Los Angeles, California 90095, United States; California Nano Systems Institute, Los Angeles, California 90095-1569, United States; orcid.org/0000-0002-8444-3348; Email: sautet@ucla.edu

ASSOCIATED CONTENT

Supporting Information. The following files are available free of charge. Computational details of the calculations, local minima included in the ensembles and SC parabolic fittings, binding energies and ΔG for ORR steps (PDF).

ACKNOWLEDGMENT

REFERENCES

(1)   Chu, S.; Majumdar, A. Opportunities and challenges for a sustainable energy future. *Nature* **2012**, *488*, 294–303.

(2) Mekhilef, S.; Saidur, R.; Safari, A. Comparative study of different fuel cell technologies. *Renew. Sustain. Energy Rev.* **2012**, *16*, 981–989.

(3) Joya, K. S.; Joya, Y. F.; Ocakoglu, K.; van de Krol, R. Water-splitting catalysis and solar fuel devices: artificial leaves on the move. *Angew. Chem. Int. Ed.* **2013**, *52*, 10426–10437.

(4) Lewis, N. S.; Nocera, D. G. Powering the planet: Chemical challenges in solar energy utilization. *Proc. Natl. Acad. Sci. U. S. A.* **2006**, *103*, 15729–15735.

(5) Halder, A.; Curtiss, L. A.; Fortunelli, A.; Vajda, S. Perspective: Size selected clusters for catalysis and electrochemistry. *J. Chem. Phys.* **2018**, *148*, 110901.

(6) von Weber, A.; Anderson, S. L. Electrocatalysis by Mass-Selected Pt_n Clusters. *Acc. Chem. Res.* **2016**, *49*, 2632–2639.

(7) Seger, B.; Kamat, P. V. Electrocatalytically Active Graphene-Platinum Nanocomposites. Role of 2-D Carbon Support in PEM Fuel Cells. *J. Phys. Chem. C* **2009**, *113*, 7990–7995.

(8) Kou, R.; Shao, Y.; Wang, D.; Engelhard, M. H.; Kwak, J. H.; Wang, J.; Viswanathan, V. V.; Wang, C.; Lin, Y.; Wang, Y.; Aksay, I. A.; Liu, J. Enhanced activity and stability of Pt catalysts

on functionalized graphene sheets for electrocatalytic oxygen reduction. *Electrochem. Commun.* **2009**, *11*, 954–957.

(9) Zhang, B. –W.; Ren, L.; Xu, Z. –F.; Cheng, N. –Y.; Lai, W. –H.; Zhang, L.; Hao, W.; Chu, S. –Q.; Wang, Y. –X.; Du, Y.; Liu, L. K.; Dou, S. –X. Atomic Structural Evolution of Single-Layer Pt Clusters as Efficient Electrocatalysts. *Small* **2021**, 2100732.

(10) Inaba, M.; Zana, A.; Quinson, J.; Bizzotto, F.; Dosche, C.; Dworzak, A.; Oezaslan, M.; Simonsen, S. B.; Kuhn, L. T.; Arenz, M. The Oxygen Reduction Reaction on Pt: Why Particle Size and Interparticle Distance Matter. *ACS Catal.* **2021**, *11*, 7144−7153.

(11) Proch, S.; Wirth, M.; White, H. S.; Anderson, S. L. Strong Effects of Cluster Size and Air Exposure on Oxygen Reduction and Carbon Oxidation Electrocatalysis by Size-Selected Pt_n (n $\leq$ 11) on Glassy Carbon Electrodes. *J. Am. Chem. Soc.* **2013**, *135*, 3073−3086.

(12) von Weber, A.; Baxter, E. T.; Proch, S.; Kane, M. D.; Rosenfelder, M.; White, H. S.; Anderson, S. L. Size-Dependent Electronic Structure Controls Activity for Ethanol Electro-Oxidation at Pt_n/Indium Tin Oxide (n = 1 to 14). *Phys. Chem. Chem. Phys.* **2015**, *17*, 17601−17610.

(13) von Weber, A.; Baxter, E. T.; White, H. S.; Anderson, S. L. Cluster Size Controls Branching Between Water And Hydrogen Peroxide Production In Electrochemical Oxygen Reduction at Pt_n/ITO. *J. Phys. Chem. C* **2015**, *119*, 11160–11170.

(14) Magee, J. W.; Zhou, W. –P.; White, M. G. Promotion of Pt surfaces for ethanol electro-oxidation by the addition of small SnO_2 nanoparticles: Activity and mechanism. *Appl. Catal. B-Environ.* **2014**, *152–153*, 397–402.

(15) Ohnuma, A.; Takahashi, K.; Tsunoyama, H.; Inoue, T.; Zhao, P.; Velloth, A.; Ehara, M.; Ichikuni, N.; Tabuchi, M.; Nakajima, A. Enhanced oxygen reduction activity of size-selected platinum subnanocluster catalysts: Pt_n (n = 3–9). *Catal. Sci. Technol.* **2022**, *12*, 1400–1407.

(16) Zandkarimi, B.; Alexandrova, A. N. Dynamics of Subnanometer Pt Clusters Can Break the Scaling Relationships in Catalysis. *J. Phys. Chem. Lett.* **2019**, *10*, 460–467.

(17) Pérez-Ramírez, J.; López, N. Strategies to break linear scaling relationships. *Nat. Catal.* **2019**, *2*, 971–976.

(18) Huang, Z. –F.; Song J.; Dou, S.; Li, X.; Wang, J.; Wang, X. Strategies to Break the Scaling Relation toward Enhanced Oxygen Electrocatalysis. *Matter* **2019**, *1*, 1494–1518.

(19) Opalka, D.; Scheurer, C.; Reuter, K. Ab Initio Thermodynamics Insight into the Structural Evolution of Working IrO_2 Catalysts in Proton-Exchange Membrane Electrolyzers. *ACS Catal.* **2019**, *9*, 4944–4950.

(20) Yoon, A.; Poon, J.; Grosse, P.; Chee, S. W.; Roldan Cuenya, B. Iodide-mediated Cu Catalyst Restructuring during CO_2 Electroreduction. *J. Mater. Chem. A* **2022**, *10*, 14041-14050.

(21) Steinmann, S. N.; Sautet, P. Assessing a First-Principles Model of an Electrochemical Interface by Comparison with Experiment. *J. Phys. Chem. C* **2016**, *120*, 5619–5623.

(22) Steinmann, S. N.; Michel, C.; Schwiedernoch, R.; Sautet, P. Impacts of electrode potentials and solvents on the electroreduction of CO_2: a comparison of theoretical approaches. *Phys. Chem. Chem. Phys.* **2015**, *17*, 13949–13963.

(23) Liu, L.; Liu, C. Origin of the overpotentials for HCOO⁻ and CO formation in the electroreduction of CO_2 on Cu(211): the reductive de-sorption processes decide. *Phys. Chem. Chem. Phys.* **2018**, *20*, 5756–5765.

(24) Baxter, E. T.; Ha, M.-A.; Cass, A. C.; Alexandrova, A. N.; Anderson, S. L. Ethylene Dehydrogenation on $Pt_{4,7,8}$ clusters on Al_2O_3: Strong Cluster-Size Dependence Linked to Preferred Catalyst Morphologies. *ACS Catal.* **2017**, *7*, 3322–3335.

(25) Zhang, Z.; Zandkarimi, B.; Munarriz, J.; Dickerson, C. E.; Alexandrova, A. N. Fluxionality of Subnano Clusters Reshapes the Activity Volcano of Electrocatalysis. *ChemCatChem* **2022**, e202200345.

(26) Ramos-Sanchez, G.; Balbuena, P. B. Interactions of platinum clusters with a graphite substrate. *Phys. Chem. Chem. Phys.* **2013**, *15*, 11950–11959.

(27) Lim, D. –H.; Wilcox, J. DFT-Based Study on Oxygen Adsorption on Defective Graphene-Supported Pt Nanoparticles. *J. Phys. Chem. C* **2011**, *115*, 22742–22747.

(28) Okamoto, Y. Density-functional calculations of icosahedral M_{13} (M = Pt and Au) clusters on graphene sheets and flakes. *Chem. Phys. Lett.* **2006**, *420*, 382–386.

(29) Qi, Q.; Liu, H.; Feng, W.; Tian, H.; Xu, H.; Huang, X. Theoretical investigation on the interaction of subnano platinum clusters with graphene using DFT methods. *Comput. Mater. Sci.* **2015**, *96*, 268–276.

(30) Ma, J.; Habrioux, A.; Luo, Y.; Ramos-Sanchez, G.; Calvillo, L.; Granozzi, G.; Balbuena, P. B.; Alonso-Vante, N. Electronic interaction be-tween platinum nanoparticles and nitrogen-doped

reduced graphene oxide: effect on the oxygen reduction reaction. *J. Mater. Chem. A* **2015**, *3*, 11891–11904.

(31) Tsunoyama, H.; Ohnuma, A.; Takahashi, K.; Velloth, A.; Ehara, M.; Ichikuni, N.; Tabuchi, M.; Nakajima, A. Enhanced oxygen reduction activity of platinum subnanocluster catalysts through charge redistribution. *Chem. Commun.* **2019**, *55*, 12603–12606.

(32) Nørskov, J. K.; Rossmeisl, J.; Logadottir, A.; Lindqvist, L.; Kitchin, J. R.; Bligaard, T.; Jónsson, H. Origin of the Overpotential for Oxygen Reduction at a Fuel-Cell Cathode. *J. Phys. Chem. B* **2004**, *108*, 17886–17892.

(33) Kristoffersen, H. H.; Veggem T.; Hansen, H. A. OH formation and H_2 adsorption at the liquid water–Pt(111) interface. *Chem. Sci.* **2018**, *9*, 6912–6921.

(34) Mathew, K.; Sundararaman, R.; Letchworth-Weaver; K.; Arias, T. A.; Hennig, R. G. Implicit solvation model for density-functional study of nanocrystal surfaces and reaction pathways. *J. Chem. Phys.* **2014**, *140*, 084106.

(35) Chang, K.; Zhang, H.; Chen, J. G.; Liu, Q.; Cheng, M. –J. Constant Electrode Potential Quantum Mechanical Study of CO_2 Electrochemical Reduction Catalyzed by N-Doped Graphene. *ACS Catal.* **2019**, *9*, 8197–8207.

(36) Goodpaster, J. D.; Bell, A. T.; Head-Gordon, M. Identification of Possible Pathways for C−C Bond Formation during Electrochemical Reduction of CO_2: New Theoretical Insights from an Improved Electrochemical Model. *J. Phys. Chem. Lett.* **2016**, *7*, 1471–1477.

(37) Melander, M. M.; Kuisma, M. J.; Christensen, T. E. K.; Honkala, K. Grand-canonical approach to density functional theory of electrocatalytic systems: Thermodynamics of solid-liquid interfaces at constant ion and electrode potentials. *J. Chem. Phys.* **2019**, *150*, 041706.

(38) Hutchison, P.; Rice, P. S.; Warburton, R. E.; Raugei, S.; Hammes-Schiffer, S. Multilevel Computational Studies Reveal the Importance of Axial Ligand for Oxygen Reduction Reaction on Fe−N−C Materials. *J. Am. Chem. Soc.* **2022**, *144*, 16524−16534.

(39) Sundararaman, R.; Goddard III, W. A.; Arias, T. A. Grand canonical electronic density-functional theory: Algorithms and applications to electrochemistry. *J. Chem. Phys.* **2017**, *146*, 114104.

(40) Smidstrup, S.; Stradi, D.; Wellendorff, J.; Khomyakov, P. A.; Vej-Hansen, U. G.; Lee, M. -E.; Ghosh, T.; Jónsson, E.; Jónsson, H.; Stokbro, K. First-principles Green's-function method for surface calculations: A pseudopotential localized basis set approach. *Phys. Rev. B* **2017**, *96*, 195309.

(41) Bonnet, N.; Morishita, T.; Sugino, O.; Otani, M. First-Principles Molecular Dynamics at a Constant Electrode Potential. *Phys. Rev. Lett.* **2012**, *109*, 266101.

(42) Nishihara, S.; Otani, M. Hybrid solvation models for bulk, interface, and membrane: Reference interaction site methods coupled with density functional theory. *Phys. Rev. B* **2017**, *96*, 115429.

(43) Basdogan, Y.; Maldonado, A. M.; Keith, J. A. Advances and challenges in modeling solvated reaction mechanisms for renewable fuels and chemicals. *WIREs Comput Mol Sci.* **2019**, e1446.

(44) Gauthier, J. A.; Ringe, S.; Dickens, C. F.; Garza, A. J.; Bell, A. T.; Head-Gordon, M.; Nørskov, J. K.; Chan, K. Challenges in Modeling Electrochemical Reaction Energetics with Polarizable Continuum Models. *ACS Catal.* **2019**, *9*, 920–931.

(45) Abidi, N.; Lim, K. R. G.; Seh, Z. W.; Steinmann, S. N. Atomistic modeling of electrocatalysis: Are we there yet? *WIREs Comput. Mol. Sci.* **2021**, 11:e1499.

(46) Campos-Roldán, C. A.; Ramos-Sánchez, G.; Gonzalez-Huerta, R. G.; Vargas García, J. R.; Balbuena, P. B.; Alonso-Vante, N. Influence of sp^3-sp^2 Carbon Nanodomains on Metal/Support Interaction, Catalyst Durability, and Catalytic Activity for the Oxygen Reduction Reaction. *ACS Appl. Mater. Interfaces* **2016**, *8*, 23260−23269.

(47) Yang, J.; Kim, S. H.; Kwak, S. K.; Song, H. –K. Curvature-Induced Metal−Support Interaction of an Islands-by-Islands Composite of Platinum Catalyst and Carbon Nano-onion for Durable Oxygen Reduction. *ACS Appl. Mater. Interfaces* **2017**, *9*, 23302−23308.

(48) Schneider, W. B.; Benedikt, U.; Auer, A. A. Interaction of platinum nanoparticles with graphitic carbon structures: A computational study. *ChemPhysChem* **2013**, *14*, 2984–2989.

(49) Poidevin, C.; Paciok, P.; Heggen, M.; Auer, A. A. High resolution transmission electron microscopy and electronic structure theory investigation of platinum nanoparticles on carbon black. *J. Chem. Phys.* **2019**, *150*, 041705.

(50) Jayabal, S.; Saranya, G.; Geng, D.; Lin, L. Y.; Meng, X. Insight into the correlation of Pt–support interactions with electrocatalytic activity and durability in fuel cells. *J. Mater. Chem. A* **2020**, *8*, 9420–9446.

(51) Duan, Z.; Henkelman, G. Atomic-Scale Mechanisms of Electrochemical Pt Dissolution. *ACS Catal.* **2021**, *11*, 14439−14447.

(52) Zandkarimi, B.; Poths, P.; Alexandrova, A. N. When Fluxionality Beats Size Selection: Acceleration of Ostwald Ripening of Sub-Nano Clusters. *Angew. Chem. Int. Ed.* **2021**, *60*, 11973–11982.

(53) Hu, X.; Chen, S.; Chen, L.; Tian, Y.; Yao, S.; Lu, Z.; Zhang. X.; Zhou, Z. What is the Real Origin of the Activity of Fe−N−C Electrocatalysts in the O_2 Reduction Reaction? Critical Roles of Coordinating Pyrrolic N and Axially Adsorbing Species. *J. Am. Chem. Soc.* **2022**, *144*, 18144−18152.

(54) Zhai, H.; Alexandrova, A. N. Ensemble-Average Representation of Pt Clusters in Conditions of Catalysis Accessed through GPU Accelerated Deep Neural Network Fitting Global Optimization. *J. Chem. Theory Comput.* **2016**, *12*, 6213−6226.

(55) Peremans, A.; Tadjeddine, A. Electrochemical deposition of hydrogen on platinum single crystals studied by infrared-visible sum-frequency generation. *J. Chem. Phys.* **1995**, *103*, 7197–7203

(56) Łosiewicz, B.; Jurczakowski, R.; Lasia, A. Kinetics of hydrogen underpotential deposition at polycrystalline platinum in acidic solutions. *Electrochim. Acta* **2012**, *80*, 292 – 301.

(57) Groves, M. N.; Malardier-Jugroot, C.; Jugroot, M. Improving Platinum Catalyst Durability with a Doped Graphene Support. *J. Phys. Chem. C* **2012**, *116*, 10548−10556.

(58) Zhai, H.; Alexandrova, A. N. Local Fluxionality of Surface-Deposited Cluster Catalysts: the Case of Pt_7 on Al_2O_3. *J. Phys. Chem. Lett.* **2018**, *9*, 1696–1702.

(59) Imaoka, T.; Toyonaga, T.; Morita, M.; Haruta, N.; Yamamoto, K. Isomerizations of a Pt_4 cluster revealed by spatiotemporal microscopic analysis. *Chem. Commun.* **2019**, *55*, 4753−4756.

(60) Shen, L.; Dadras, J.; Alexandrova, A. N. Pure and Zn-doped Pt clusters go flat and upright on MgO(100). *Phys. Chem. Chem. Phys.* **2014**, *16*, 26436–26442.

(61) Shang R.; Steinmann, S. N.; Xu, B. –Q.; Sautet, P. Mononuclear Fe in N-doped carbon: computational elucidation of active sites for electrochemical oxygen reduction and oxygen evolution reactions. *Catal. Sci. Technol.* **2020**, *10*, 1006–1014.

(62) Zhang, Z.; Zandkarimi, B.; Alexandrova, A. N. Ensembles of metastable states govern heterogeneous catalysis on dynamic interfaces. *Acc. Chem. Res.* **2020**, *53*, 447–458.

(63) Zhai, H.; Alexandrova, A. N. Fluxionality of Catalytic Clusters: When It Matters and How to Address It. *ACS Catal.* **2017**, *7*, 1905–1911.

(64) Zhang, Z.; Cui, Z. -H.; Jimenez-Izal, E. ; Sautet, P. ; Alexandrova, A. N. Hydrogen Evolution on Restructured B-Rich WB: Metastable Surface States and Isolated Active Sites. *ACS Catal.* **2020**, *10*, 13867–13877.

(65) Lavroff, R. H.; Morgan, H. W. T; Zhang, Z.; Poths, P.; Alexandrova, A. N. Ensemble representation of catalytic interfaces: soloists, orchestras, and everything in-between. *Chem. Sci.* **2022**, *13*, 8003–8016.

(66) Hansen, H. A.; Viswanathan, V.; Nørskov, J. K. Unifying Kinetic and Thermodynamic Analysis of 2 e⁻ and 4 e⁻ Reduction of Oxygen on Metal Surfaces. *J. Phys. Chem. C* **2014**, *118*, 6706–6718.

(67) Benedikt, U.; Schneider, W. B.; Auer, A. A. Modelling electrified interfaces in quantum chemistry: constant charge vs. constant potential. *Phys. Chem. Chem. Phys.* **2013**, *15*, 2712–2724.

(68) Ping, Y.; Nielsen, R. J.; Goddard III, W. A. The Reaction Mechanism with Free Energy Barriers at Constant Potentials for the Oxygen Evolution Reaction at the IrO_2 (110) Surface. *J. Am. Chem. Soc.* **2017**, *139*, 149−155.

(69) Yang, J. A computational study on the electrified Pt(111) surface by the cluster model. *Phys. Chem. Chem. Phys.* **2019**, *21*, 6112–6125.

(70) Hoogers, G.; Thompsett, D. The role of catalysis in proton exchange membrane fuel cell technology. *CATTECH* **1999**, *3*, 106.

(71) Kulkarni, A.; Siahrostami, S.; Patel A.; Nørskov, J. K. Understanding Catalytic Activity Trends in the Oxygen Reduction Reaction. *Chem. Rev.* **2018**, *118*, 2302–2312.

(72) Debe, M. K. Electrocatalyst approaches and challenges for automotive fuel cells. *Nature* **2012**, *486*, 43–51.

(73) Pt_5 clusters over glassy carbon have been found to be active towards ORR, as described in reference 15.